Phosphorus Retention and Hydraulic Performance in Borrow Sand-Based Wastewater Soil Treatment Units in Impermeable Settings: Case Study in Abitibi-Témiscamingue, Québec

Coauthors: Sorour Sheibani[a]*, Michelle Nasrallah[a], Benoît Courcelles[a], Eric Rosa[b], Brahim Maylal[b] and Dominique Claveau-Mallet[a]

[a]Department of Civil, Geological & Mining Engineering, Polytechnique Montréal, 2900 Boulevard Édouard-Montpetit, Montréal, Québec H3T 1J4, Canada.

[b]Groundwater Research Group (GRES), Research Institute on Mines and Environment (RIME), Université du Québec en Abitibi-Témiscamingue (UQAT), 341 Rue Principale N, Amos, Québec J9T 2L8, Canada.

*Corresponding author

1. Soil type estimations

Québec's guidelines classify soil as very permeable, permeable, lowly permeable, and impermeable, each with a specific range of hydraulic conductivity: (i) very permeable ($K > 4\times10^{-5}$ m/s), (ii) permeable (2×10^{-6} m/s $< K < 4\times10^{-5}$ m/s), (iii) lowly permeable (6×10 7 m/s $< K < 2\times10^{-6}$ m/s), and (iv) impermeable ($K < 6\times10^{-7}$ m/s) where K is the hydraulic conductivity of the in situ soils. Various methods exist to determine soil type, including defining hydraulic conductivity through *in situ* and laboratory permeability tests and subsequently categorizing soil types based on the obtained hydraulic conductivity (MELCCFP, 2017). Another approach involves using the soil texture triangle to estimate soil type based on its particle size distribution (MELCCFP, 2017). Fig. S1 shows the correlation between the texture triangle and the 4 soil types. In this study, the samples collected from the field were plotted on the triangle as seen in Fig. S1 and their soil types were estimated using this method.

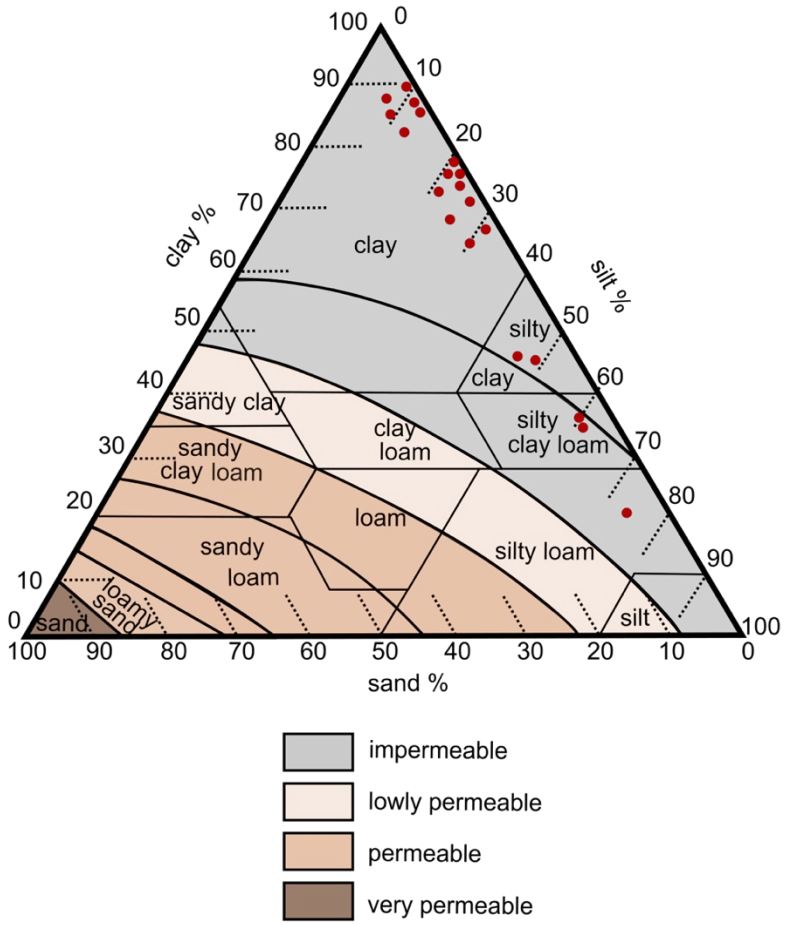

Figure S1- Correlation between the texture triangle and impermeable, lowly permeable, permeable and very permeable soil (MELCCFP, 2017) and the plotted natural soil samples.

2. Sanitary inspection sampling points

The following figure shows the location of the ditch, the polishing bed leading to the ditch and sampling points in sanitary field inspections.

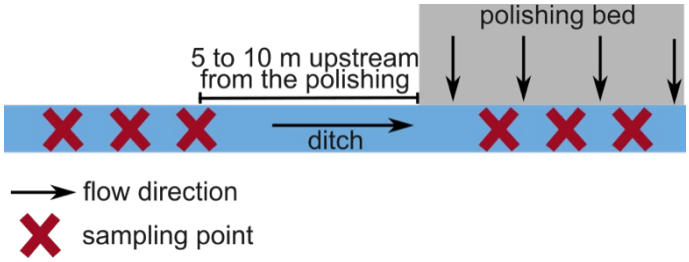

Figure S2- Plan of sampling points in sanitary inspections.

3. Inspected systems

Inspected systems are listed in the following table.

Table S1- Characteristics of inspected systems (type of distribution of wastewater from the pipes, number of bedrooms of residences, number of residents, area, occupation rate, installation year, and category of the septic system).

System number	Type of distribution	Number of Bedroom	Residents	Area (m^2)	Estimated hydraulic load (m^3/d)	Occupation rate	Installation year	Category
1	Gravity-fed	3	2	16	0.54	33%	2009	2
2	Low-pressure	3	3	16	0.81	50%	2018	2
3	Low-pressure	3	2	16	0.54	33%	2006	3
4	Low-pressure	4	4	22	1.08	50%	2018	2
5	Low-pressure	5	4	27	1.08	40%	2014	1
6	Gravity-fed	4	2	22	0.54	25%	2005	3
7	Gravity-fed	4	2	22	0.54	25%	2019	1
8	Low-pressure	4	2	22	0.54	25%	2018	2
9	Gravity-fed	3	2	16	0.54	33%	2018	2
10	Low-pressure	2	2	11	0.54	50%	2017	2
11	Low-pressure	2	1	11	0.27	25%	2015	3
12	Gravity-fed	3	2	16	0.54	33%	2019	1

13	Low-pressure	6	6	32	1.62	50%	2020	3
14	Low-pressure	2	2	11	0.54	50%	2018	2
15	Low-pressure	4	2	22	0.54	25%	2017	2
16	Low-pressure	3	2	16	0.54	33%	2011	2
17	Low-pressure	3	4	16	1.08	67%	2019	2
18	Low-pressure	4	2	22	0.54	25%	2020	3
19	Gravity-fed	4	5	22	1.35	63%	2017	1
20	Low-pressure	1	2	7	0.54	100%	2020	3
21	Gravity-fed	5	6	27	1.62	60%	2020	2
22	Gravity-fed	4	4	22	1.08	50%	2018	1
23	Gravity-fed	3	3	16	0.81	50%	2013	2
24	Low-pressure	4	4	22	1.08	50%	2013	3
25	Low-pressure	4	2	22	0.54	25%	2015	1
26	Low-pressure	1	2	7	0.54	100%	2012	3

The hydraulic loads of the systems were estimated based on the number of residents and the wastewater production of 270 L/d (MELCCFP, 2017). Systems 7 and 16 demonstrated ground surface flooding.

4. Gravity-fed vs low-pressure distribution systems

In a gravity-fed system, a preferential flow forms at the nearest orifice to the supply pipe and therefore, the flow does not distribute evenly through pipes. On the other hand, low-pressure

distributing systems distribute the flow almost evenly through the network by pressurizing. In reality, pipes are perforated, and the discharge comes out of holes with small areas. In a low-pressure distribution system, the water leaves the pipes upwards. In the modelling section, low-pressure distribution systems were simulated. To ease the numerical convergence, a uniform inflow through the upper half of the lateral area of pipes was considered.

5. S1 and S2 meeting specifications

To make sure that the specifications are met, the particle size distributions of 2 sand samples were obtained according to ASTM C136 (ASTM International, 2020) and presented in Fig. S3.

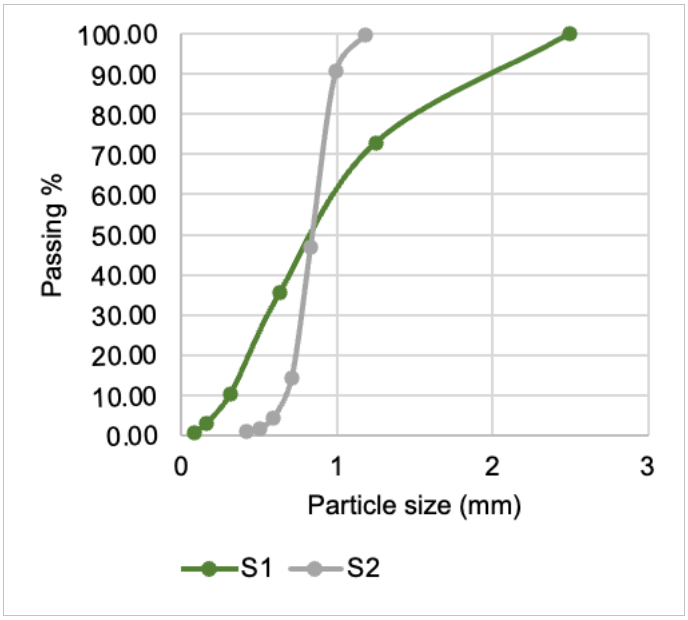

Figure S3- Particle distribution curves of S1 and S2.

Table S2 shows that both S1 and S2 met all specifications.

Table S2- Sands specifications and their validations for S1 and S2.

Specification	**Validation for S1**	**Validation for S2**
0.25 mm < d_{10} <1 mm	d_{10} = 0.31	d_{10} = 0.66
C_u <4.5	C_u = 3.30	C_u = 1.33
Particles smaller than 80 μm < 3 %	Particles smaller than 80 μm = 0.57 %	No particles smaller than 80 μm
Particles bigger than 2.5 mm < 20%	No particles bigger than 2.5 mm	No particles bigger than 2.5 mm

6. Polishing beds plans

Fig. S4 exhibits the plans for rectangular and square polishing beds associated with 6-bedroom residences.

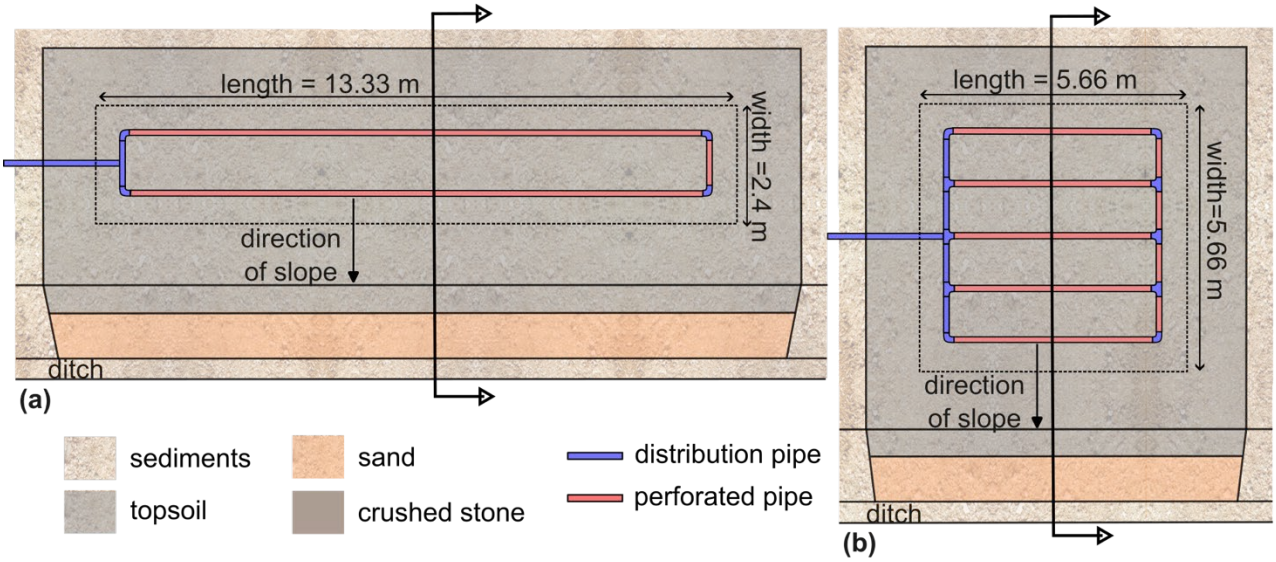

Figure S4- Plan of polishing beds designed for 6-bedroom residences. (a) rectangular polishing bed and (b) square polishing bed. The dashed line shows the boundaries of the crushed stone layer.

7. 3D modeling of polishing bed vs 2D

Fig. S5 illustrates the 3D simulation of model 1 in day 360. The horizontal blue plane represents the water table within the polishing bed and the P plume in Fig. S5a indicates the isosurface corresponding to a 4 mg/l P concentration (80% of the inlet concentration). The contaminant plume saturated the crushed stone layer and extended downslope through the sand layer toward the ditch. While the equivalent 2D model yielded a lifetime of 110 days (Table 5), a relatively small content of P dispersed perpendicular to the slope resulted in a longer yet comparable lifetime of 160 days in the 3D model. The minimum unsaturated thickness in the 3D model was 0.61 m which is merely 1 cm greater than that of the 2D model (0.6 m, as in Table 5). Fig. S5b displays the P concentration

contour in a cross-section extracted from the 3D model exhibiting a strong similarity to the configuration of the equivalent 2D model (Fig. 6a). The 3D simulation demanded a substantial computation time of 46 hours, highlighting the practical advantage of opting for 2D simulations running in less than an hour.

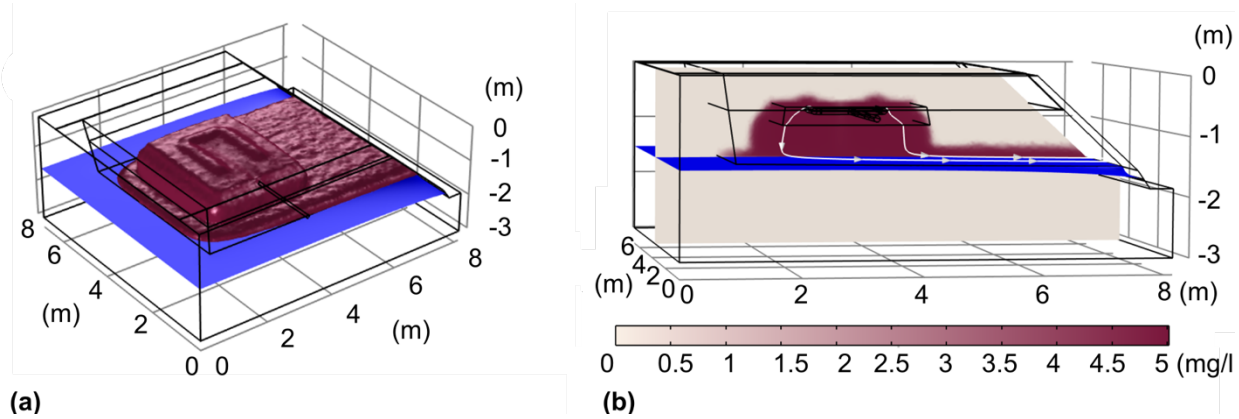

Figure S5- Model 1 3D simulation in day 360. (a) Isosurface of 4 mg/l of P and water table and (b) water table, contour map of P concentration and streamlines in a cross-section.

Dispersion along the omitted dimension (the dimension perpendicular to the STU's slope) is not accounted for in the 2D model. This simplification is valid when flow and transport primarily occur within the modeled plane, but it may introduce inaccuracies in cases where lateral spreading is significant. Despite the overall agreement between 2D and 3D results, 3D modeling remains essential in situations where lateral contaminant dispersion cannot be neglected, such as in non-uniform subsurface flow conditions, heterogeneous media, or when assessing contaminant migration toward nearby water bodies or infrastructure. Although 3D simulations offer greater detail, their high computational cost (46 hours compared to under an hour for 2D) limits their practicality unless lateral transport is a key focus.

8. No flow boundaries in numerical modelling

In general, two types of no-flow boundaries were implemented; bottom no-flow boundaries and side no-flow boundaries. The bottom no-flow boundaries are deep enough to not affect the hydraulic integrity and transport of phosphorus. No-flow side-boundaries can imply the impermeability in the sediments layer which is realistic since the sediments layer is clayey in

general. Additionally, the main hydraulic behavior of the polishing beds was in a way that highly permeable sand layer did not allow for water accumulation but instead helped forming an outlet flow towards the ditch. Also, the phosphorus (P) plume never approached these boundaries. Therefore, the location of the no-flow side-boundaries is not influential regarding the above-mentioned pattern.

9. Numerical meshing

Triangular mesh was built automatically with COMSOL Multiphysics. In 2D modelling, mesh size varied from 1.8×10^{-4} m to 0.02 m and in 3D modelling mesh size varied from 0.001m to 0.09 m. Different mesh sizes, spanning from twice as coarse to twice as fine as the size of the final mesh, were tested and revealed grid convergence, as the results remained consistent regardless of variations in mesh size.

10.Justification of porous media parameters used for modelling

Topsoil was considered to be loamy, representing a natural cover for the culture of grass, as commonly observed in backyards. Hodnett and Tomasella, (2002) tested 771 soils and derived values of van Genuchten parameters as well as porosity and residual water content. We used the average parameters they suggested for loam for topsoil. Topsoil's hydraulic conductivity was set in the range of permeable soil according to Québec's guidelines (MELCCFP, 2017).

Based on the particle size distribution of S1 and S2 sands, their hydraulic conductivities were estimated using Kozney-Carman, Hazen and Breyer formulas. These empirical formulas were shown to give the most precise estimations among available empirical formulas (Odong, 2007). The values of 1.22×10^{-3} and 7.88×10^{-3} m/s were obtained for S1 and S2, respectively. The value used in simulations is the average hydraulic conductivity of the two sands. For other properties of the sand, we referred to the study by Benson et al. (2014) in which the measured hydraulic properties of fine, medium, and coarse sand were presented based on their particle sizes. We used average values for sand samples with d_{60} and d_{10} values that compare to the sands used in our work. The results of the sieve test conducted on the 20 samples collected from the field revealed that the sediment layer is impermeable. The imposed hydraulic conductivity for this layer was set to a low value suggesting impermeability. Other hydraulic properties of fine sediments were the values presented by (Hodnett and Tomasella, 2002) for clayey soil.

Crushed stone is composed of 20 mm particles. The hydraulic conductivity of crushed stone with 20 mm particles was estimated from (Judge, 2013) and the porosity was taken from (Al- Fawzy and Al- Mohammed, 2019). The residual water content was set to zero since the particles are large. Furthermore, since the crushed stone used in the infiltration beds is washed prior to usage, fine particles are not included, and the coarse particles produce low suction which means that the α parameter is relatively large. Also, the value of n, for soils with limited breadth of the particle size distribution, tends to be relatively high (Benson et al., 2014). Here, the highest value with which the models converge was used.

The runoff layer was addressed according to Chapuis (2009) with its hydraulic conductivity being 10^4 times greater than most permeable media in the model (sand), as suggested by Chapuis (2009).

11. Analysis of natural soil covering

Fig. S6 shows the particle size distribution curve of the 20 samples taken from the field.

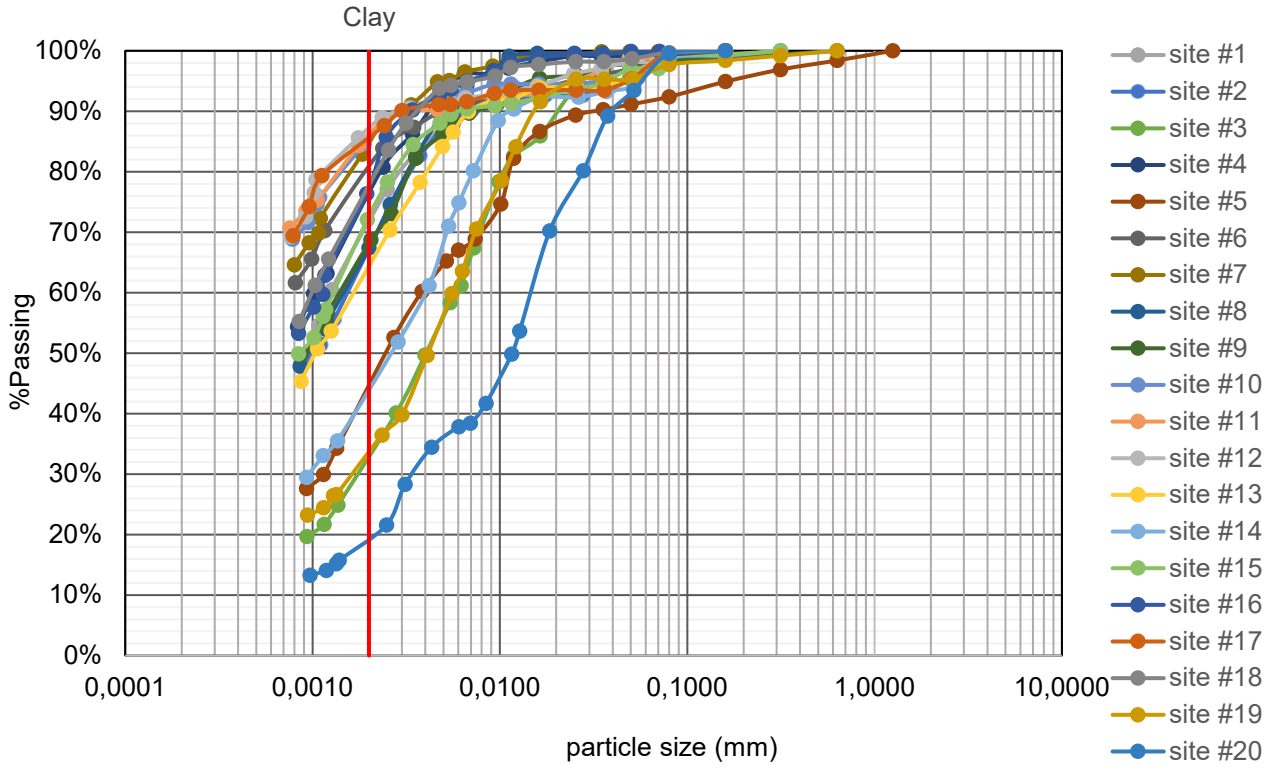

Figure S6- Particle size distribution curves of the 20 soil samples.

12. pH in adsorption batch test

The pH in the initial solutions ranged from 5.4 to 5.8 (acidic solutions). After agitation, the pH measured in samples containing S2 were still in the range of 4.8 – 5.0 (acidic) while the pH of samples with S1 reached the range of 6.8 - 7.1 (alkaline). This difference could be due to the mineral compositions of different sands. Measured pH values are reported in Table S3.

Table S3- Initial pH of samples, and final pH of blank sample, samples with S1 and samples with S2.

Target concentrations mg P/L	**Initial pH**	**Final pH**		
		Blank samples	**Samples with S1**	**Samples with S2**
20.00	5.40	5.37	ND*	4.85
15.00	5.34	5.34	6.82	ND*
10.00	5.47	Nd*	7.05	4.97
5.00	5.64	5.61	ND*	4.97
2.00	5.77	5.81	ND*	ND*

Not determined (ND)

The pH was not measured for all the samples after the rotation period because the quantities of certain samples were limited and necessary to be able to make the required dilutions for concentration calculations.

13. Evolution of P plume

In Fig. S7, contour maps show the progression of P concentration in the polishing bed of model 1 throughout its lifespan. Similar patterns were observed in other models.

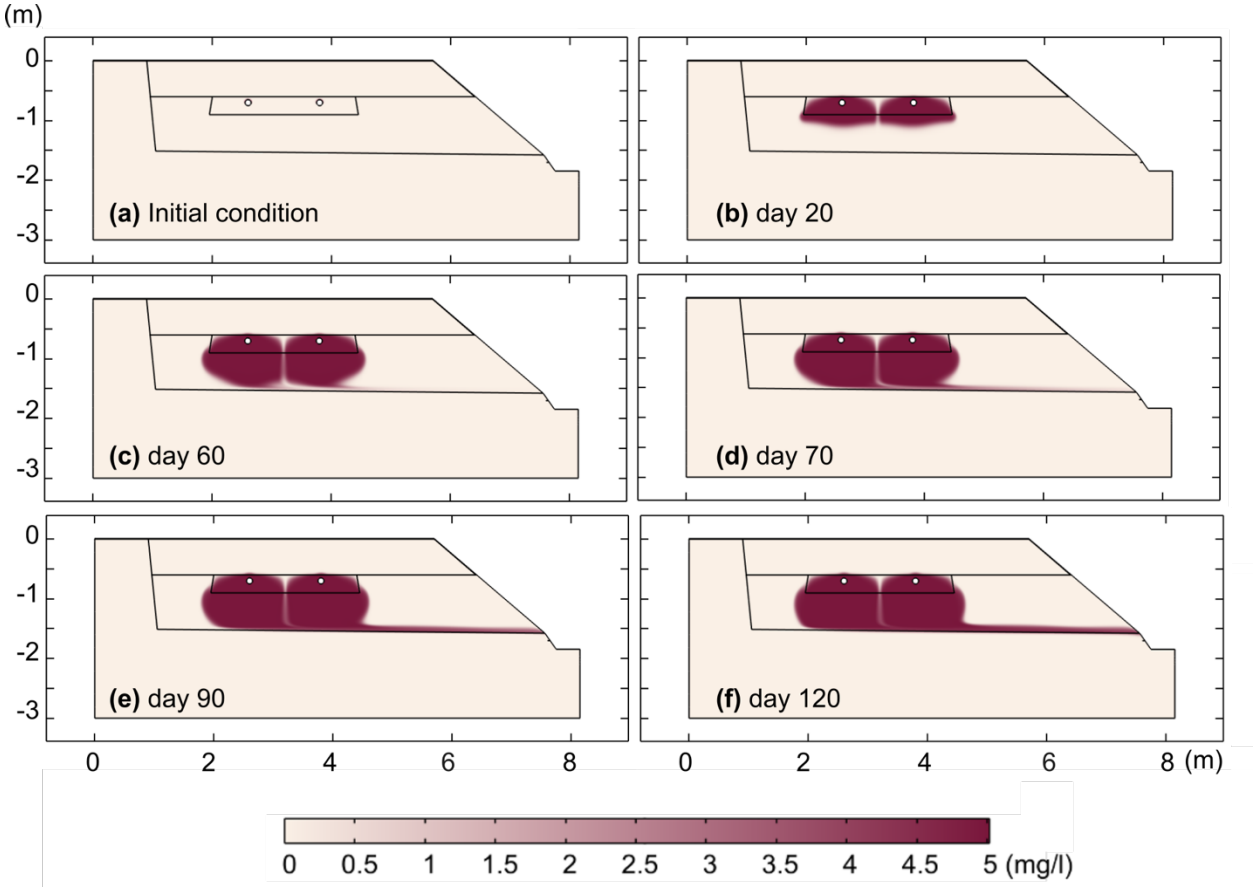

Figure S7- Contour map of P concentration in (a) initial condition, (b) day 20, (c) day 60, (d) day 70, (e) day 90, and (f) day 120 of operation of polishing bed in model 1.

References

Al- Fawzy, A.M., Al- Mohammed, F.M., 2019. Dissipation of Energy of Flow by Conventional Type of Gabion Weir. IOP Conf Ser Mater Sci Eng 584, 012038. https://doi.org/10.1088/1757-899X/584/1/012038

ASTM International, 2020. ASTM C136M, Standard Test Method for Sieve Analysis of Fine and Coarse Aggregates.

Benson, C.H., Chiang, I., Chalermyanont, T., Sawangsuriya, A., 2014. Estimating van Genuchten Parameters α and n for Clean Sands from Particle Size Distribution Data, in: From Soil Behavior Fundamentals to Innovations in Geotechnical Engineering. American Society of Civil Engineers, Reston, VA, pp. 410–427. https://doi.org/10.1061/9780784413265.033

Chapuis, R.P., 2009. Numerical modeling of reservoirs or pipes in groundwater seepage. Comput Geotech 36, 895–901. https://doi.org/10.1016/j.compgeo.2009.01.005

Hodnett, M.G., Tomasella, J., 2002. Marked differences between van Genuchten soil water-retention parameters for temperate and tropical soils: a new water-retention pedo-transfer functions developed for tropical soils. Geoderma 108, 155–180. https://doi.org/10.1016/S0016-7061(02)00105-2

Judge, A., 2013. Measurement of the hydraulic conductivity of gravels using a laboratory permeameter and silty sands using field testing with observation wells. University of Massachusetts Amherst.

MELCCFP, 2017. Ministère de l'Environnement, de la Lutte contre les changements climatiques, de la Faune et des Parcs, Guide pour l'étude des technologies conventionnelles de traitement des eaux usées d'origine domestique, chapitre 3.

Odong, J., 2007. Evaluation of empirical formulae for determination of hydraulic conductivity based on grain-size analysis. Journal of American Science 54–60.